Acta Crystallographica Section D
Biological Crystallography
ISSN 0907-4449

Structure of cytochrome c_7 from *Desulfuromonas acetoxidans* at 1.9 Å resolution

Mirjam Czjzek,[a]* Pascal Arnoux,[a] Richard Haser[b] and William Shepard[c]†

[a]Laboratoire d'Architecture et de Fonction des Macromolécules Biologiques, CNRS et Université Aix Marseille I and II, Marseille, 31 Chemin Joseph-Aiguer, 13402 Marseille CEDEX 20, France, [b]Institut de Biologie et de Chimie des Protéines, CNRS Lyon, 7 Passage du Vercors, 69367 Lyon CEDEX 07, France, and [c]Laboratoire pour l'Utilisation du Rayonnement Electromagnetique, Bâtiment 209d, BP 34, Centre Universitaire Paris-Sud, 91898 Orsay CEDEX, France

† Present address: European Synchrotron Radiation Facility, 6 Rue Jules Horowitz, BP 220, 38043 Grenoble CEDEX, France.

Correspondence e-mail: czjzek@afmb.cnrs-mrs.fr

Received 20 December 2000
Accepted 19 February 2001

PDB Reference: cytochrome c_7, 1hh5.

Multihaem cytochromes play a key role in electron-transport reactions in the periplasm of sulfate- and sulfur-reducing bacteria. The redox proteins grouped in the c_3 superfamily also display metal-reducing activities, which make them interesting biotechnological tools. The crystal structure of the fully oxidized cytochrome c_7 from *Desulfuromonas acetoxidans* has been solved by combined molecular-replacement and MAD methods. The structure has been refined at 1.9 Å resolution to an R value of 19.1% ($R_{\rm free}$ = 24.3%) and includes three haems and 116 water molecules. The protein displays the cytochrome c_3 fold in a highly minimized form, while haem 2 and the surrounding protein environment are missing. The geometry of haem packing and of the haem axial ligands and propionates are described and compared with that of c_3 cytochromes. The crystal structure is compared with the solution structure recently obtained by NMR methods and with its homologue cytochromes of the c_3 superfamily. Comparison of the high number of available structures makes it possible to analyze the structural role of the few highly conserved residues, in addition to the cysteines and histidines that link the porphyrin rings and the Fe atoms to the protein chain.

1. Introduction

Cytochrome c_7 is known to be the smallest representative of the multihaem cytochrome c_3 superfamily (Bruschi, 1994), with 68 amino acids and three haem groups (Ambler, 1971). This class of cytochromes, defined by Ambler as type III (Ambler, 1980), was first identified in the 1950s by Postgate (1954) and Ishimoto *et al.* (1954). A large number of multihaem cytochromes with different haem contents, varying from three to 16 haem groups per polypeptide chain, are currently known. The crystal structures of tetrahaem (Czjzek, Payan, Guerlesquin *et al.*, 1994; Haser, Pierrot *et al.*, 1979; Higuchi *et al.*, 1984, 1994; Matias *et al.*, 1993, 1996; Nørager *et al.*, 1999), octahaem (Czjzek *et al.*, 1996, Frazão *et al.*, 1999) and nonahaem (Matias *et al.*, 1999) cytochromes c_3 demonstrate that these proteins are variants and/or multimers of the tetrahaem cytochrome c_3 motif. The recently obtained NMR solution structure of cytochrome c_7 (Assfalg *et al.*, 1998) revealed that this cytochrome is no exception and, as has been predicted by sequence alignments, it is the haem 2 and the corresponding protein chain that are missing in this shortest version of cytochromes c_3.

The main characteristic of these small soluble cytochromes is the bishistidinal axial ligation of all the haem groups in the molecule, which present low, albeit different, redox potentials (between −50 and −400 mV). Although the amino-acid

Table 1
Data-collection and processing statistics.

Wavelength	R_{sym}† (%)	R_{ano}‡ (%)	f'	f''	Overall redundancy	Completeness (%)	N_{ref}§ unique	Resolution (Å)
λ_1, 1.8035 (remote1)	5.0	5.0	−3.02	0.5¶	3.2	83.8	577	27–4.02
λ_2, 1.7405 (inflection)	6.6	6.8	−10.34	4.86	3.1	82.8	628	27–3.85
λ_3, 1.7342 (peak)	5.9	7.1	−4.86	5.44	3.1	83.6	635	27–3.82
λ_4, 1.6668 (remote2)	4.3	6.1	−2.12	5.46	3.1	87.3	712	27–3.69
Native, 1.5418 (outer shell 2.0–1.9 Å)	8.2 (18.2)				3.6	92 (90)	5213	13–1.9

† R_{sym} $|I - \langle I\rangle|/\sum\langle I\rangle$. ‡ $R_{ano} = \sum|I(+) - I(-)|/\sum\langle I\rangle$. § N_{ref}, number of reflections. ¶ The f' and f'' values for λ_1 were kept constant while the f' and f'' values for all other wavelengths were refined (suggestion in the *SHARP* manual).

Table 2
Statistics of phasing and phase combination.

Phasing statistics.

	FOM†	Resolution range (Å)	No. of phased reflections
FOM of MAD phases (*SHARP*)	0.716	27–3.69	729
FOM after *DM* on MAD phases	0.746	27–3.69	729
Molecular-replacement phases	0.812	13–2.1	3910
σ_A-weighted model phases	0.816	13–2.1	3910

Phase combination.

Resolution range (Å)	Centric				Acentric			
	N‡	Comb§	MAD	Part/St¶	*N*	Comb	MAD	Part/St
8.51–6.17	25	0.9295	0.7105	0.7316	46	0.9521	0.8549	0.7804
6.17–5.09	28	0.8553	0.5899	0.7432	69	0.9427	0.8285	0.8651
5.09–4.42	29	0.9167	0.5509	0.7797	99	0.9508	0.8224	0.8828
4.42–3.97	34	0.8131	0.4049	0.7954	112	0.9468	0.6737	0.9026
3.97–3.63	15	0.8455	0.2794	0.8373	72	0.9034	0.4902	0.8600

Overall FOM after phase combination (resolution range 27–2.0 Å).

	N	FOM
Centric	731	0.70053
Non-centric	3377	0.80518
Total	4108	0.78656

† Figure of merit. ‡ No. of reflections with combined phases. § Combined FOM. ¶ FOM of partial structure.

composition, sequence homology, formal charges and isoelectric points of these cytochromes may be very different, the haem packing geometry is highly conserved in all the proteins studied. The highly conserved core of these redox proteins, consisting of the four (or three) haem cluster, the cysteines covalently linking the haems to the polypeptide chain and the axial ligands, is primarily responsible for the observed thermostability of these cytochromes (Dolla *et al.*, 1999; Florens *et al.*, 1995).

Cytochrome c_7 is the most abundant cytochrome in the periplasm of *D. acetoxidans* and, like most of the cytochromes c_3, is most probably reduced physiologically by an [NiFe]-hydrogenase (Brugna *et al.*, 1999). The *Desulfuromonas* bacteria cannot reduce sulfate but requires sulfur as an obligatory respiratory electron acceptor, using acetate as oxidizable substrate. The oxidation of acetate to CO_2 is stoichiometrically linked to the reduction of elemental sulfur to sulfide. More recently, it has been suggested that cytochrome c_7 could be involved in the coupled oxidation of acetate and dissimilatory reduction of Fe^{III} and Mn^{IV} (Roden & Lovley, 1993) to obtain energy for growth of these bacteria. This interesting property of reductive precipitation of highly toxic metals (Lovley, 1993), also observed for other cytochromes c_3, makes them accessible tools for the bioremediation of waters and soils contaminated by heavy metals. Cytochrome c_7 has been extensively examined by NMR methods in the past (Assfalg *et al.*, 1998, 1999; Banci *et al.*, 1996; Coutinho *et al.*, 1996; Moura *et al.*, 1984), recently leading to a solution structure (Assfalg *et al.*, 1998). However, no crystal structure has been determined to date. We report here the three-dimensional crystal structure of cytochrome c_7 at 1.9 Å resolution obtained by the combination of phases of a MAD experiment and molecular replacement with the NMR structures (PDB codes 1new and 2new).

2. Methods and materials

2.1. Data collection and processing

The protein was extracted and purified as previously described (Probst *et al.*, 1977). The crystals were grown in hanging drops by mixing 4 µl of protein (9 mg ml^{-1} in 20 m*M* Tris pH 7.6) with 2 µl of reservoir solution containing 20–22% PEG 1000, 0.1 *M* Tris buffer at pH 7.6. These conditions are close to those previously described (Haser, Payan *et al.*, 1979). Microseeding was necessary in order to obtain suitable crystals for the X-ray diffraction experiments. The crystals belong to space group $P2_12_12_1$ and have unit-cell parameters $a = 37.55$, $b = 44.10$, $c = 45.08$ Å. The native data set was collected from a single crystal on a Rigaku rotating-anode generator (Cu $K\alpha$), equipped with a MAR Research imaging-plate detector at room temperature, while the MAD data sets were collected from a single crystal on beamline D2AM (Fanchon *et al.*, 1995; Roth *et al.*, 1992) at the ESRF. The crystal for the MAD experiment was cryocooled by transferring it into a solution of mother liquor containing 20% ethylene glycol prior to freezing in an N_2 stream at 100 K. The unit-cell parameters changed to $a = 37.19$, $b = 43.83$, $c = 44.80$ Å. The data were collected at four wavelengths (Table 1) chosen from the XANES spectrum at the iron *K* edge measured directly from the protein crystal. No attempt was made to optimize the quality of the anomalous signal by aligning the crystal along any crystallographic axes in order to record Bijvoet reflection pairs on the same image. All data were processed with *XDS* (Kabsch, 1988) and scaled with *SCALA* (Collaborative Computational Project, Number 4, 1994). The data-collection and processing statistics are given in Table 1.

2.2. Structure determination

The structure was solved by the molecular-replacement method using the *AMoRe* program (Navaza, 1994). The first set of atomic coordinates of the NMR solution structures with PDB code 1new was used as search model. The initial *R* factor and correlation coefficient obtained were 0.475 and 0.340, respectively, in the resolution range 13.0–3.8 Å. The correlation coefficient for the next solution was about 0.10 lower. After one cycle of torsion-angle refinement using the slow-cooling protocol as implemented in *CNS* (Brunger *et al.*, 1998) the *R* factor fell to 24% ($R_{\rm free}$ = 38%). However, the $2F_o - F_c$ and $F_o - F_c$ maps calculated at this stage of the procedure were not very instructive and still had significant discontinuities.

The MAD data collected on D2AM for a crystal of cytochrome c_7 were only available to 3.8 Å resolution owing to the geometrical arrangement of the goniometer and CCD detector on D2AM combined with the long wavelength at the iron edge (1.74 Å). For the same reasons, the X-ray diffraction data sets were insufficiently complete (83–87% complete). The Patterson maps were extremely noisy and could not be deconvoluted. However, the use of the iron positions obtained from the molecular-replacement solution gave a set of phases with a mean FOM value of 0.716 with the program *SHARP* (de La Fortelle & Bricogne, 1997). This led to 729 phased reflections (Table 2). The maps calculated with the experimental phases were of very low resolution and did not resolve the structure.

In order to enhance the maps obtained from the molecular-replacement solution, the phases obtained from the model were improved by solvent flattening and then combined with the MAD phases by Bricogne's adaptation of Sim's weighting scheme (Bricogne, 1976) using the option 'combine part' from the program *SIGMAA* (Collaborative Computational Project, Number 4, 1994). The phase-combination statistics are given in Table 2. As can be seen in Fig. 1, the phase combination led to clearly defined electron-density maps and the model correction and refinement were subsequently straightforward. The refinement was performed with the program *CNS* (Brunger *et al.*, 1998). The water molecules were placed on inspection of the electron-density maps and three residues (Thr5, Thr14 and Ser55) were modelled in two alternate conformers. When refining against the native data set at 1.9 Å resolution collected at room temperature, the *R* factor converged to 19.1% (20–1.9 Å, 5213 reflections) for the final model with the inclusion of 116 water molecules. The final refinement statistics are summarized in Table 3.

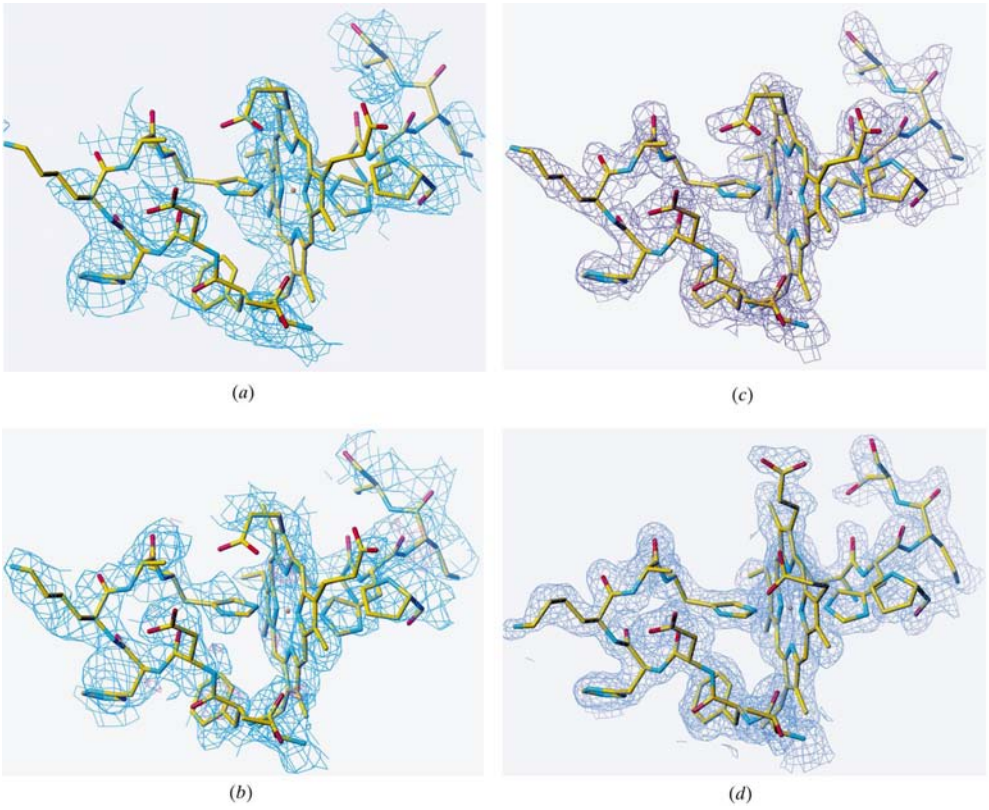

Figure 1
A portion of the electron-density map of the region around haem 3 showing the axial ligands, calculated with the phases obtained at different stages of the phasing procedure. The structural model in (*a*), (*b*) and (*c*) is the NMR-solution structure placed with respect to the crystal form by molecular replacement after one cycle of simulated-annealing refinement with *CNS*. All maps are contoured at the 1σ level. This figure, as well as Figs. 4 and 5, were produced with *TURBO-FRODO* (Roussel & Cambillau, 1991). (*a*) Electron-density map calculated at 3.8 Å resolution with the phases resulting from the MAD experiment as obtained by the program *SHARP* (de La Fortelle & Bricogne, 1997) and *DM* (Collaborative Computational Project, Number 4, 1994). (*b*) Map calculated at 2.5 Å resolution with the phases resulting from the solution found by molecular replacement after one cycle of refinement using a simulated-annealing protocol as implemented in *CNS* (Brunger *et al.*, 1998) and subsequent solvent flattening with *DM* (Collaborative Computational Project, Number 4, 1994). The $2F_o - F_c$ map (blue) is contoured at a 1σ level, while the $F_o - F_c$ positive peaks (red) are contoured at a 2σ level. (*c*) $2F_o - F_c$ map calculated with the phases resulting from the phase combination of the phases as in (*a*) and (*b*) obtained with the program *SIGMAA* (Collaborative Computational Project, Number 4, 1994). (*d*) Final $2F_o - F_c$ map calculated with the phases of the final structural model (superposed in stick representation) at 1.9 Å resolution.

3. Results and discussion

3.1. Molecular structure and haem packing geometry

The cytochrome c_7 has a flattened triangular form (Figs. 2*a* and 2*b*) with a molecular size of approximately 21 × 24 × 32 Å^3. The final model includes all 68 amino acids (three residues have been modelled in two alternate

conformations), three haem groups and 116 water molecules. To facilitate structural comparison, the same haem nomenclature has been adopted as in Assfalg *et al.* (1999). According to the convention for cytochromes c_3, the haems present in cytochrome c_7 are called haem 1, haem 3 and haem 4 in sequential order. The stereochemical quality of the refined structure was verified using the program *PROCHECK* (Laskowski *et al.*, 1993), which shows that 87.9% of the residues are in the most favoured region of the Ramachandran plot and 10.3% are in the additional allowed region. The overall structure resembles that of tetrahaem cytochrome c_3, where the region corresponding to haem 2 is simply replaced by a straight polypeptide connection. Analysis of the temperature factors as a function of residue number (colour coded in the representation of Fig. 2*b*) shows that the *B*-factor values are highly correlated to the r.m.s. deviation, as obtained for the same residue number in the NMR solution structures with respect to a mean structure (Fig. 2*c*). Overall, the model obtained from the crystal structure superposes well with the structure determined by NMR methods. Some differences, however, concern the haem geometry and the orientation of the haem axial ligands (Table 4). In particular, the histidine-plane angles with respect to each other and with respect to the haem plane show some striking differences, while the overall geometry of the haem packing fits quite well (Table 4). The most marked difference concerns His53, the fifth axial ligand of haem 3, where the hydrogen bond formed with Pro59 (Table 5) is completely missing in the NMR solution structure and the histidine plane takes a different orientation. To a minor extent, the same is true for His30 and His66. The regions for the residues 31–33 and 57–60 have been reported to lack NMR constraints (Assfalg *et al.*, 1998, 1999), which makes these regions difficult to determine by NMR methods. They have the highest r.m.s.d. values within the family of NMR structures and this most likely explains the discrepancies between the reported NMR structures and the present crystallographic structure. Moreover, the regions around the haem groups (*i.e.* the histidine ligands) in the fully oxidized cytochrome structure are particularly difficult to obtain by NMR methods, since the oxidized iron is paramagnetic and broadens the NMR lines. The orientation of the histidine plane with respect to the haem plane is known to influence the redox potential of the haem iron (Guigliarelli *et al.*, 1990). Compared with those observed in the homologous cytochromes c_3 (Czjzek, Payan & Haser, 1994; Nørager *et al.*,

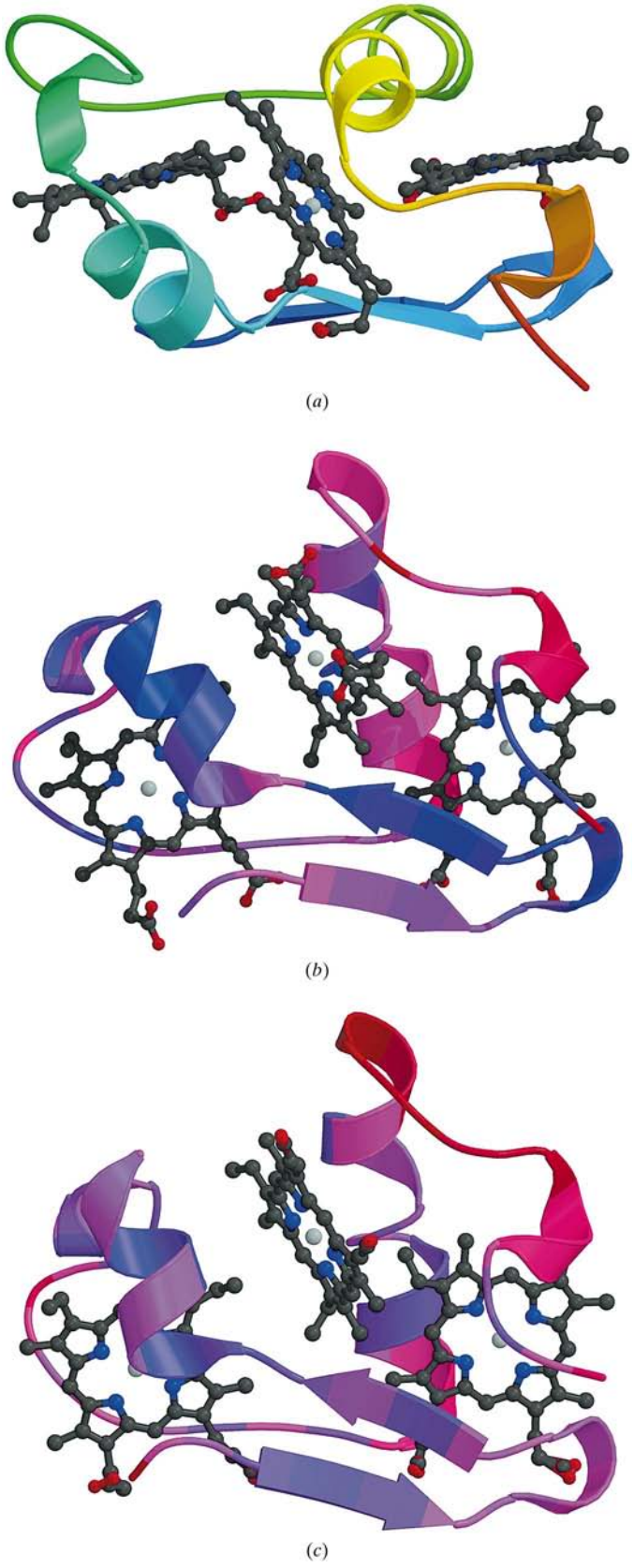

Figure 2
Ribbon representation of the structural model of cytochrome c_7. The figure was produced with *Molscript* (Kraulis, 1991) and *Raster3D* (Merritt & Murphy, 1994). (*a*) Structural model of c_7 as observed in the crystal structure showing an orientation in which this cytochrome appears as a flattened object. The protein backbone is gradually coloured from blue (N-terminus) to orange (C-terminus). The haem groups from the left to the right are haems 1, 3 and 4. (*b*) Structural model obtained from the crystal structure in an orientation perpendicular to that in (*a*). The cytochrome has a near-triangular form. The region of each residue is coloured according to its mean *B*-factor value. In the range 5–15 Å^2 the regions are coloured blue, the regions in pink vary from 15 to 25 Å^2 and for *B*-factor values between 25 and 35 Å^2 the region is coloured red. (*c*) Ribbon representation of the mean NMR solution structure of c_7. The colours represent the r.m.s. deviation from the mean structure for a given residue, as calculated from the deposited files in the PDB, 1new and 2new.

Table 3
Refinement statistics.

Resolution range (Å)	14.0–1.9
σ cutoff	$F_{obs} < 0.01$
R_{cryst} (%) (No. of reflections)	19.1 (4671)
R_{free} (%) (5% of reflections)	24.2 (542)
No. of non-H protein atoms	505
No. of heteroatoms	129
No. of solvent atoms	116
R.m.s. deviation from ideal geometry	
Bond lengths (Å)	0.008
Bond angles (°)	4.2
Dihedrals (°)	26.3
Impropers (°)	1.7
Average B factors (Å^2)	24.12
All atoms	24.12
Main-chain atoms	20.31
Side-chain atoms	22.35
Haem atoms	16.25
Water molecules	44.5
Luzzati coordinate error (Å)	0.21
σ_A coordinate error (Å)	0.11
Ramachandran outliers	1
Residues in most favourable regions (%)	87.9

1999), the values obtained from the crystal structure of oxidized cytochrome c_7 are very similar and reflect well the high conservation of the haem-core and haem-coordination geometry (see Table 4). Throughout the determined structures, exceptions are only observed for the values of the histidines that are the sixth axial ligand of haem 1, haem 3 and haem 4, respectively. In occurrence, the plane of the histidine which is the sixth axial ligand of haem 4 in cytochrome c_3 from *Desulfomicrobium baculatus* Norway (Dmbn) is oriented in an almost perpendicular manner to those of the equivalent histidines in all the other cytochromes c_3. It had been postulated that this change in orientation was the result of a highly conserved tyrosine residue missing in cytochrome c_3 from Dmbn that shields the sixth axial ligand from the solvent in all other cytochromes c_3 (Czjzek, Payan & Haser, 1994).

Table 4
Haem packing geometry and angles between the axial ligands of cytochrome c_7 in the crystal and in solution, as well as compared with two c_3-type cytochromes.

	Oxidized crystal	Oxidized NMR†	Reduced NMR†	c_3 Dmbn crystal‡	cc$_3$ Dmbn crystal‡
Fe–Fe distances (Å)					
Haem 1–haem 3	11.53	12.0	11.9	10.9	11.2
Haem 1–haem 4	19.28	18.3	18.9	17.3	17.7
Haem 3–haem 4	12.59	11.8	12.5	12.7	12.2
Angle between haem planes (°)					
Haem 1–haem 3	81	30.6	41.0	84.5	80.4
Haem 1–haem 4	8	1.8	10.7	30.5	27.5
Haem 3–haem 4	77	68.4	55.9	75.9	71.2
Angles between Fe atoms (°)					
Haem 1–haem 3–haem 4	106	100.3	101.2	92.3	97.7
Haem 3–haem 4–haem 1	35	40.2	38.2	40.2	39
Haem 3–haem 1–haem 4	39	39.4	40.6	47.5	43.3
Angle between His planes (°)					
His17–His30 (haem 1)	78.8	52.4	55.4	5	7.1
His20–His53 (haem 3)	31.4	52.2	26.5	25.6	12.2
His45–His66 (haem 4)	82.9	61.7	52.9	77.2	0.2
Angle between His plane and vector NA–NC of the haem group (°)					
His17 (haem 1)	−57.3	−58.0	−49.6	54.8	43.2
His30 (haem 1)	42.7	41.2	37.0	59.8	50.3
His20 (haem 3)	−17.7	−86.1	−102.4	−18.4	−26.9
His53 (haem 3)	49.2	59.7	43.7	44.0	39.1
His45 (haem 4)	−51.7	−34.6	−22.0	−53.0	38.4
His66 (haem 4)	31.3	27.7	46.5	49.8	38.6

† Results as reported in Assfalg *et al.* (1999). ‡ Results as reported in Czjzek, Payan & Haser (1994).

However, site-directed mutagenesis experiments on dimeric octahaem cytochrome c_3 (cc$_3$) from Dmbn, where this tyrosine Tyr73 has been replaced by a glutamic acid (the equivalent residue in cytochrome c_3 from Dmbn) show that this mutation did not influence the histidine orientation. On the contrary,

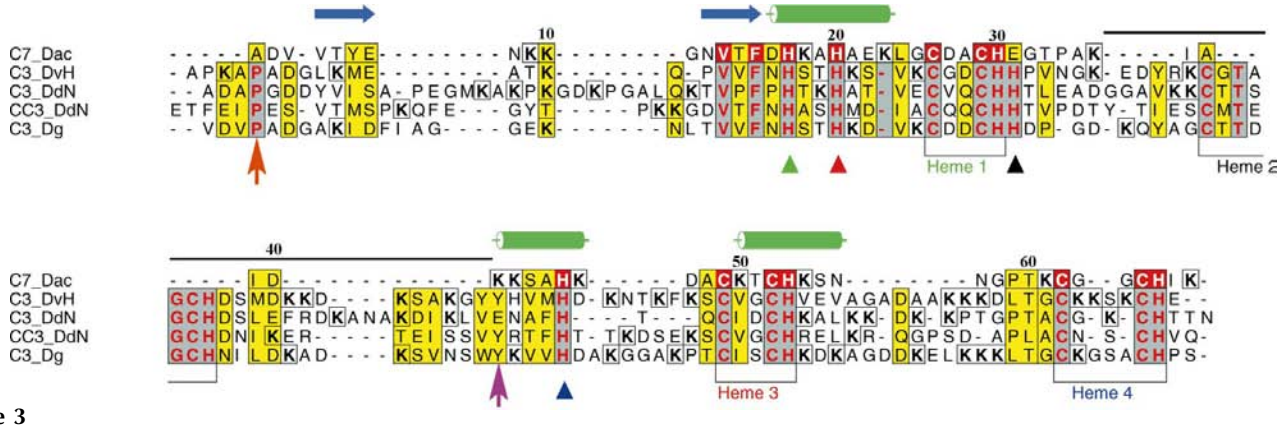

Figure 3
Sequence alignment of selected cytochromes from the c_3 superfamily. The figure was produced with *Alscript* (Barton, 1993). C7_Dac, trihaem cytochrome c_7 from *Desulforomonas acetoxidans*; C3_DvH, tetrahaem cytochrome c_3 from *Desulfovibrio vulgaris* Hildenborough; C3_DdN, tetrahaem cytochrome c_3 from *Desulfomicrobium baculatus* Norway; CC3_DdN, octahaem haem cytochrome c_3 from *Desulfomicrobium baculatus* Norway; C3_Dg, tetrahaem cytochrome c_3 from *Desulfovibrio gigas*. The alignment shows secondary-structure elements of the c_3 fold (β-strands as blue arrows, α-helices as green cylinders). The numbering corresponds to the sequence of cytochrome c_7. The residues involved in haem attachments are boxed underneath and an arrowhead, in the same colour as the haem name, designates the histidine that is the sixth axial ligand. Yellow boxes denote sites of high sequence similarity, while red and grey boxes denote highly conserved residues throughout the c_3 superfamily. The orange arrow shows a highly conserved proline residue in the N-terminal region, missing in cytochrome c_7. The magenta arrow shows the site of a tyrosine residue, discussed in the text.

the mutation Tyr73Glu in cc_3 perturbs the interaction with the periplasmic [NiFeSe] hydrogenase (Czjzek *et al.*, 1996). Another feature defining the histidine-plane orientation is the hydrogen-bonding pattern involving the $N^{\delta1}$ atoms of the histidine residues (Table 5). The pattern is highly conserved throughout the cytochrome c_3 structures (Czjzek, Payan & Haser, 1994; Matias *et al.*, 1996) and involves conserved water molecules close to haem 1 which are also present in cytochrome c_7.

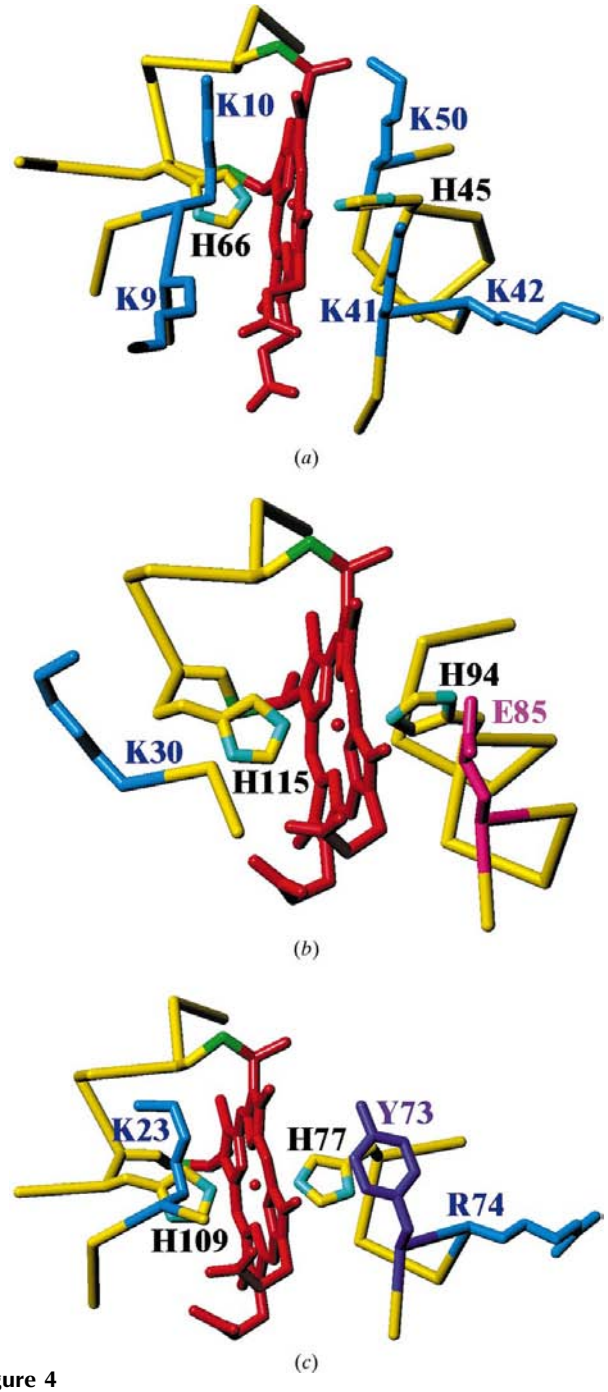

Figure 4
Stick representation of a view onto the surface-exposed edge of haem 4 in cytochrome c_7 (*a*) in the crystal structure, (*b*) cytochrome c_3 from Dmbn and (*c*) cytochrome cc_3 from Dmbn. The residue shielding the histidine that is the sixth axial ligand of haem 4 against the solvent is of different nature in these three examples.

Table 5
Hydrogen-bonding pattern of the histidine residues, fifth and sixth axial ligands of the Fe atoms.

Secondary hydrogen bonds are given in italics.

	Histidine residue	Hydrogen-bonded residue	Distance (Å)
Haem 1	His17 $N^{\delta1}$	Ow 105	2.63
	His17 $N^{\delta1}$	Ala1 O	3.28
	His30 $N^{\delta1}$	Ow 145	2.86
	His30 $N^{\delta1}$	Ala35 O	3.19
Haem 3	His20 $N^{\delta1}$	Asp16 O	2.95
	His20 $N^{\delta1}$	Ow 122	3.88
	His53 $N^{\delta1}$	Pro59 O	2.72
	His53 $N^{\delta1}$	Cys49 O	3.97
Haem 4	His45 $N^{\delta1}$	Ow 133	3.08
	His45 $N^{\delta1}$	Lys41 O	3.58
	His66 $N^{\delta1}$	Gly11 O	2.77
	His66 $N^{\delta1}$	Asn8 OD1	3.31

Interestingly, the sixth axial ligand of haem 4 in the crystal structure of cytochrome c_7 has the same orientation as in cytochrome c_3 of Dmbn and the conserved tyrosine is also missing in the sequence of cytochrome c_7 (Fig. 3). Structurally, a lysine residue takes the place of the tyrosine, shielding the histidine from the solvent (Fig. 4). This is obviously a second example where a changed orientation of the plane of the histidine that is the sixth axial ligand of haem 4 is coupled to the lack of a highly conserved residue. However, as has been shown above by the mentioned mutagenesis studies, the conserved tyrosine residue is apparently not the only factor governing the histidine-plane orientation.

Another example of the histidine planes having an exceptional different orientation is encountered for His17 in cytochrome c_7 and the equivalent His24 in the acidic cytochrome c_3 from *Desulfovibrio africanus* (Nørager *et al.*, 1999). The sequence alignments in Nørager *et al.* (1999) and in Fig. 3 reveal that these cytochromes are both missing an extremely well conserved proline residue close to the N-terminus. This proline residue, which precedes the first β-strand, has its ring plane approximately parallel to the histidine that is the sixth axial ligand of haem 1 in all other structures reported for the superfamily cytochrome c_3, including the octahaem cytochromes c_3 (Frazão *et al.*, 1999; Czjzek *et al.*, 1996) and the nonahaem cytochrome (Matias *et al.*, 1999). These examples seem to point out that, together with other factors, the highly conserved proline and tyrosine residues are to some extent responsible for the His-plane orientation. Furthermore, these two residues, the proline in the N-terminal region and the tyrosine in the C-terminal region, are each facing the solvent, shielding the neighboring histidine on the most solvent-exposed edge of the corresponding haem group. This could implicate that these residues are important either for electron transport and/or for the interaction of the concerned haem groups and the interacting physiological partners. Indeed, numerous studies have demonstrated that in cytochromes c_3 it is haem 4 which lies in the site interacting with the periplasmic

hydrogenase (Brugna *et al.*, 1998; Dolla *et al.*, 1991; Guerlesquin *et al.*, 1985; Haladjian *et al.*, 1987). As in other cytochromes c_3, the region around haem 4 in cytochrome c_7 contains a cluster of lysine residues (see Fig. 4*a*) responsible for a global positive charge around haem 4. We therefore conclude again that haem 4 is the most probable site of electrostatic interaction of cytochrome c_7 with its physiological partners.

3.2. Crystal packing and intermolecular interactions

In the crystal each molecule makes intermolecular contacts with nine neighbours. The crystal consists of a lattice of close-packed molecules interwoven with extremely small canals of solvent (about 5 Å in diameter), corresponding to a volume fraction of 32%. The asymmetric unit contains one molecule and the arrangement of the molecules in the crystal packing creates two intermolecular close contacts that bring the respective haem groups close to each other. Haem 1 of one molecule faces haem 4 of a symmetry-related molecule (Fe—Fe distance 19.3 Å; Fig. 5*a*) and haem 4 of the same molecule faces haem 3 of another symmetric molecule (Fe—Fe distance 16.7 Å; Fig. 5*b*). These distances are of the same order as those observed for the intramolecular Fe—Fe distances of the haem groups (Table 4). Since the driving forces for crystallization are governed by intermolecular protein–protein attraction, which are most often of electrostatic nature, and the same is true for the interaction of redox proteins with their physiological partners along the electron-transport pathway, these interacting regions may be of functional relevance. Furthermore, kinetic studies have demonstrated a cooperative process for some cytochromes c_3, which is most easily explained by intermolecular interactions (Brugna *et al.*, 1998).

The first contact region, bringing haem 1 close to haem 4 of a symmetry-related molecule, is interesting because the propionate groups of haem 1 are facing two lysine residues, Lys41 and Lys42, in proximity to haem 4, but no direct salt bridge is formed (Fig. 5*a*). The involvement of lysine residues in the interaction of multihaem *c*-type cytochromes with their redox partners has been long established (Dolla *et al.*, 1991; Stewart *et al.*, 1989).

A very interesting feature can be observed at the other interacting region, involving Lys10 and Lys62. Here, haem 4 of one molecule is facing haem 3 of a symmetry-related molecule and the haem planes are almost parallel to each other (Fig. 5*b*). This parallel but offset arrangement is often observed in electron-transport proteins containing haem groups, such as cytochrome c_{554} (Iverson *et al.*, 1998) and the photosynthetic reaction centre, between the two bacteriochlorophyll groups that form the special pair (Deisenhofer *et al.*, 1985). All in all, only a limited number of haem packing motifs have been observed (Iverson *et al.*, 1998) and they may reflect favourable haem–haem interactions that facilitate electron-transfer processes. The shortest distance between the haem edges of haem 3 and 4 in this interaction region is formed by the surface-exposed cysteine–vinyl covalent bonds of each involved haem group (SG–CM, 4.4 Å; SG–SG,

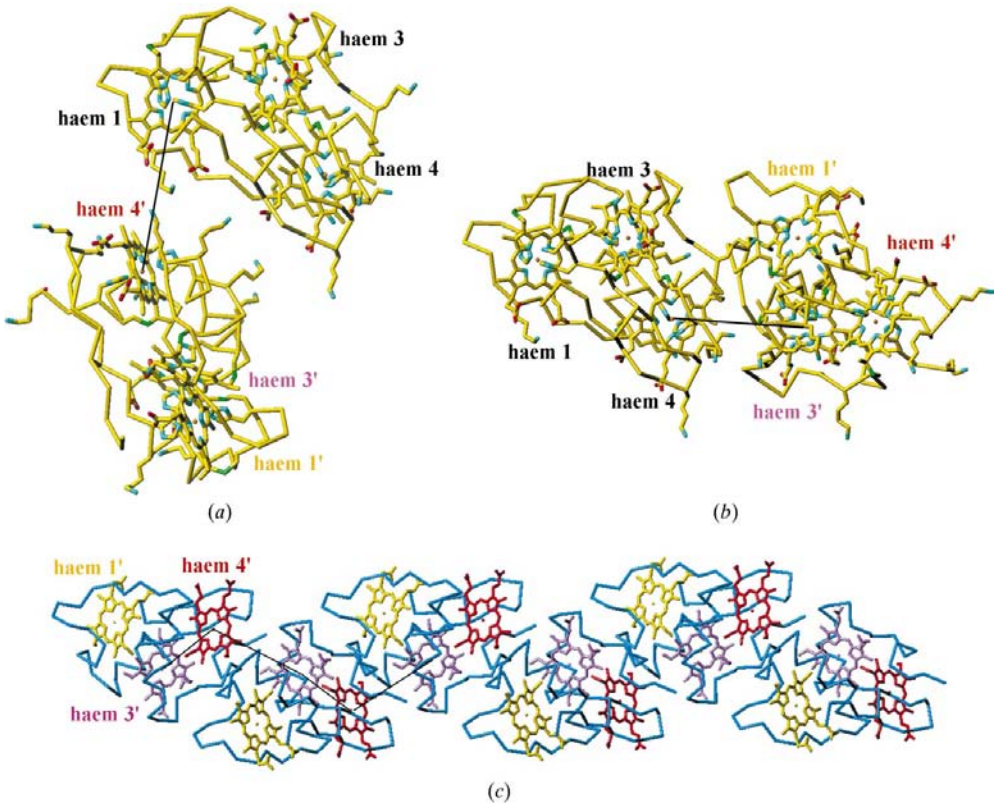

Figure 5
Intermolecular contacts in the crystal packing bringing haem groups of symmetry-related molecules into close proximity. (*a*) The N-terminal region and haem 1 of one molecule are facing haem 4 of a symmetry-related molecule. The Fe—Fe distance is 19.3 Å; the closest contact is observed between the haem propionate groups of haem 1 and Lys41 and Lys42 of the symmetry-related molecule. (*b*) A crystal packing contact bringing haem 4 of one molecule edge-to-edge with haem 3 of a symmetry-related molecule. The Fe—Fe distance is 16.7 Å. Hydrophobic contacts between the haem edges are of the order of magnitude of 5 Å. A short distance between the S atoms of the cysteines covalently linking the respective haem group may play an important role in electron-transport reactions. (*c*) The contact described in (*b*) forms a zig-zagging chain through the crystal, alternating intramolecular haem contacts between haem 3 and haem 4 (12.6 Å) and intermolecular contacts between haem 4 and haem 3 (16.7 Å). This electron-transport chain might have physiological implications.

3 Å). This close contact between cysteine–vinyl linkages intriguingly resembles that observed at the dimer interface of the octahaem cytochrome c_3 (Czjzek *et al.*, 1996) between the two haem 1s of each monomer. Recently, a very similar contact between a cysteine–vinyl linkage on one side and a cysteine–Fe bond of a Fe_4S_4 centre on the other has also been observed in the electron-transfer complexes of ferredoxin (Morelli, Dolla *et al.*, 2000) and [NiFe]-hydrogenase with the cytochrome c_{553} (Morelli, Czjzek *et al.*, 2000) of *Desulfovibrio* species. All these examples favour the assumption that this close contact is one possible relevant arrangement for favourable electron transfer between haem groups. It is noteworthy that thin solid films of cytochrome c_3 from *Desulfovibrio vulgaris* Miyazaki display a particularly low resistance when exposed to electrodes (Kimura *et al.*, 1979). Moreover, kinetic studies of this type of cytochrome have shown that they reduce their physiological partner, the hydrogenase, in a cooperative process (Brugna *et al.*, 1998). This cooperativity was explained by cytochrome–cytochrome interactions forming a 'chain' of c_3-type cytochromes. When analyzing the crystal packing, it can be noticed that this close contact between haems 4 and haem 3 of an adjacent molecule expands throughout the crystal in a one-dimensional zig-zagging chain (Fig. 5*c*). It is therefore possible to conclude that this contact could lead to an intermolecular electron-transfer pathway between cytochrome c_7 molecules.

We thank Mireille Bruschi for gratefully providing us with purified protein samples. We are equally indebted to Philippe Carpentier for his scientific assistance on beamline D2AM at the ESRF, Grenoble.

References

Ambler, R. P. (1971). *FEBS Lett.* **18**, 351–353.

Ambler, R. P. (1980). *From Cyclotrons to Cytochromes*, edited by A. B. Robinson & N. O. Kaplan, pp. 263–279. London/New York: Academic Press.

Assfalg, M., Banci, L., Bertini, I., Bruschi, M., Giudici-Orticoni, M. T. & Turano, P. (1999). *Eur. J. Biochem.* **266**(2), 634–643.

Assfalg, M., Banci, L., Bertini, I., Bruschi, M. & Turano, P. (1998). *Eur. J. Biochem.* **256**(2), 261–270.

Banci, L., Bertini, I., Bruschi, M., Sompornpisut, P. & Turano, P. (1996). *Proc. Natl Acad. Sci. USA*, **93**(25), 14396–14400.

Barton, G. J. (1993). *Protein Eng.* **6**(1), 37–40.

Bricogne, G. (1976). *Acta Cryst.* A**32**, 832–847.

Brugna, M., Giudici-Orticoni, M. T., Spinelli, S., Brown, K., Tegoni, M. & Bruschi, M. (1998). *Proteins*, **33**(4), 590–600.

Brugna, M., Nitschke, W., Toci, R., Bruschi, M. & Giudici-Orticoni, M. T. (1999). *J. Bacteriol.* **181**(17), 5505–5508.

Brunger, A. T., Adams, P. D., Clore, G. M., DeLano, W. L., Gros, P., Grosse-Kunstleve, R. W., Jiang, J. S., Kuszewski, J., Nilges, M., Pannu, N. S., Read, R. J., Rice, L. M., Simonson, T. & Warren, G. L. (1998). *Acta Cryst.* D**54**(5), 905–921.

Bruschi, M. (1994). *Methods Enzymol.* **243**, 140–155.

Collaborative Computational Project, Number 4 (1994). *Acta Cryst.* D**50**, 760–763.

Coutinho, I. B., Turner, D. L., Liu, M. Y., LeGall, J. & Xavier, A. V. (1996). *J. Biol. Inorg. Chem.* **1**, 305–311.

Czjzek, M., Guerlesquin, F., Bruschi, M. & Haser, R. (1996). *Structure*, **4**(4), 395–404.

Czjzek, M., Payan, F., Guerlesquin, F., Bruschi, M. & Haser, R. (1994). *J. Mol. Biol.* **243**(4), 653–667.

Czjzek, M., Payan, F. & Haser, R. (1994). *Biochimie*, **76**, 546–553.

Deisenhofer, J., Epp, O., Miki, K., Huber, R. & Michel, H. (1985). *Nature (London)*, **318**, 618–624.

Dolla, A., Arnoux, P., Protasevich, I., Lobachov, V., Brugna, M., Giudici-Orticoni, M. T., Haser, R., Czjzek, M., Makarov, A. & Bruschi, M. (1999). *Biochemistry*, **38**(1), 33–41.

Dolla, A., Leroy, G., Guerlesquin, F. & Bruschi, M. (1991). *Biochim. Biophys. Acta*, **1058**(2), 171–177.

Fanchon, E., Ferrer, J.-L., Kahn, R., Berthet, C. & Roth, M. (1995). *ESRF Newsl.* **24**, 6–7.

Florens, L., Bianco, P., Haladjian, J., Bruschi, M., Protasevich, I. & Makarov, A. (1995). *FEBS Lett.* **373**(3), 280–284.

Frazão, C., Sieker, L., Sheldrick, G., Lamzin, V., LeGall, J. & Carrondo, M. A. (1999). *J. Biol. Inorg. Chem.* **4**(2), 162–165.

Guerlesquin, F., Noailly, M. & Bruschi, M. (1985). *Biochem. Biophys. Res. Commun.* **130**(3), 1102–1108.

Guigliarelli, B., Bertrand, P., More, C., Haser, R. & Gayda, J. P. (1990). *J. Mol. Biol.* **216**(1), 161–166.

Haladjian, J., Bianco, P., Guerlesquin, F. & Bruschi, M. (1987). *Biochem. Biophys. Res. Commun.* **147**(3), 1289–1294.

Haser, R., Payan, F., Bache, R., Bruschi, M. & Le Gall, J. (1979). *J. Mol. Biol.* **130**(1), 97–98.

Haser, R., Pierrot, M., Frey, M., Payan, F., Astier, J. P., Bruschi, M. & Le Gall, J. (1979). *Nature (London)*, **282**(5741), 806–810.

Higuchi, Y., Akutsu, H. & Yasuoka, N. (1994). *Biochimie*, **76**(6), 537–545.

Higuchi, Y., Kusunoki, M., Matsuura, Y., Yasuoka, N. & Kakudo, M. (1984). *J. Mol. Biol.* **172**(1), 109–139.

Ishimoto, M., Koyama, J. & Nagai, Y. (1954). *Bull. Chem. Soc. Jpn*, **27**, 564–565.

Iverson, T. M., Arciero, D. M., Hsu, B. T., Logan, M. S. P., Hooper, A. B. & Rees, D. C. (1998). *Nature Struct. Biol.* **5**(11), 1005–1012.

Kabsch, W. (1988). *J. Appl. Cryst.* **18**, 916–924.

Kimura, K., Nakahara, Y., Yagi, T. & Inokuchi, H. (1979). *J. Chem. Phys.* **70**, 3317–3321.

Kraulis, P. (1991). *J. Appl. Cryst.* **24**, 946–950.

La Fortelle, E. de & Bricogne, G. (1997). *Methods Enzymol.* **276**, 472–494.

Laskowski, R. A., MacArthur, M. W., Moss, D. S. & Thornton, J. M. (1993). *J. Appl. Cryst.* **26**, 283–291.

Lovley, D. R. (1993). *Annu. Rev. Microbiol.* **47**, 263–290.

Matias, P. M., Frazão, C., Morais, J., Coll, M. & Carrondo, M. A. (1993). *J. Mol. Biol.* **234**(3), 680–699.

Matias, P. M., Morais, J., Coelho, R., Carrondo, M. A., Wilson, K., Dauter, Z. & Sieker, L. (1996). *Protein Sci.* **5**(7), 1342–1354.

Matias, P. M., Saraiva, L. M., Soares, C. M., Coelho, A. V., LeGall, J. & Carrondo, M. A. (1999). *J. Biol. Inorg. Chem.* **4**(4), 478–494.

Merritt, E. A. & Murphy, M. E. P. (1994). *Acta Cryst.* D**50**, 869–873.

Morelli, X., Czjzek, M., Hatchikian, C. E., Bornet, O., Fontecilla-Camps, J. C., Palma, N. P., Moura, J. J. & Guerlesquin, F. (2000). *J. Biol. Chem.* **275**(30), 23204–23210.

Morelli, X., Dolla, A., Czjzek, M., Palma, P. N., Blasco, F., Krippahl, L., Moura, J. J. & Guerlesquin, F. (2000). *Biochemistry*, **39**(10), 2530–2537.

Moura, J. G., Moore, G. R., Williams, R. J., Probst, I., Legall, J. & Xavier, A. V. (1984). *Eur. J. Biochem.* **144**(3), 433–440.

Navaza, J. (1994). *Acta Cryst.* A**50**, 157–163.

Nørager, S., Legrand, P., Pieulle, L., Hatchikian, C. & Roth, M. (1999). *J. Mol. Biol.* **290**(4), 881–902.

Postgate, J. R. (1954). *Biochem. J.* **56**, xi.

Probst, I., Bruschi, M., Pfennig, N. & Le Gall, J. (1977). *Biochim. Biophys. Acta*, **460**(1), 58–64.
Roden, E. E. & Lovley, D. R. (1993). *Appl. Environ. Microbiol.* **59**, 734–742.
Roth, M., Ferrer, J.-L., Simon, J.-P. & Geissler, E. (1992). *Rev. Sci. Instrum.* **63**(1), 1043–1046.
Roussel, A. & Cambillau, C. (1991). *TURBO-FRODO*. Silicon Graphics Geometry Partners Directory, Silicon Graphics, Mountain View, CA, USA.
Stewart, D. E., Legall, J., Moura, I., Moura, J. J., Peck, H. D. Jr, Xavier, A. V., Weiner, P. K. & Wampler, J. E. (1989). *Eur. J. Biochem.* **185**(3), 695–700.